Pflügers Archiv - European Journal of Physiology (2018) 470:481–490
https://doi.org/10.1007/s00424-017-2091-y

ION CHANNELS, RECEPTORS AND TRANSPORTERS

Heterogeneous functional expression of the sustained inward Na^+ current in guinea pig sinoatrial node cells

Futoshi Toyoda[1] · Ding Wei-Guang[1] · Hiroshi Matsuura[1]

Received: 25 September 2017 / Revised: 8 November 2017 / Accepted: 21 November 2017 / Published online: 3 December 2017

Abstract

The sustained inward Na^+ current (I_{st}) identified in the sinoatrial node (SAN) cell has been suggested to play a pivotal role in cardiac pacemaking. However, the composition of cells in the SAN is heterogeneous and cell-to-cell variability in the magnitude of I_{st} remains to be fully characterized. The present study investigated the current density of I_{st} in morphologically different types of pacemaker cells dissociated from guinea pig SAN. I_{st} was preferentially detected in spontaneously active spindle or spider-shaped cells, but was less well expressed in larger-sized elongated spindle-type cells and practically absent in clearly striated atrial-like cells, despite clear expression of the funny current (I_f). The current density of I_{st} in spindle and spider cells varied from 0.7 to 1.6 pA pF^{-1} and was significantly reduced in non-beating cells with similar morphologies. By linear regression analysis, we identified a positive correlation between the current densities of I_{st} and the L-type Ca^{2+} current ($I_{Ca,L}$), which was specifically observed in spindle and spider cells. These cells exhibited a more negative voltage for half maximal $I_{Ca,L}$ activation than atrial-like cells, suggesting a variable ratio between $Ca_V1.2$- and $Ca_V1.3$-mediated $I_{Ca,L}$ in SAN cells. Consistent single-cell transcript measurements confirmed a higher relative expression of $Ca_V1.3$, which activates at more negative potentials, in spindle cells than in atrial-like cells. Taken together, these results can be interpreted as indicating that I_{st} plays a specific role in primary pacemaker cells and that its presence is closely correlated with functional levels of $Ca_V1.3$-mediated $I_{Ca,L}$.

Keywords Sinoatrial node cells · Sustained inward current · L-type Ca^{2+} current · $Ca_V1.3$ · Cellular heterogeneity

Abbreviations

$I_{Ca,L}$	L-type Ca^{2+} current
I_f	Hyperpolarization-activated cation current
I_{st}	Sustained inward current
SAN	Sinoatrial node

Introduction

Understanding the pacemaker mechanism in cardiac sinoatrial node (SAN) cells is a long-standing problem [18]. Many ion channels and electrogenic transporters as well as intracellular Ca^{2+} have so far been identified as potential contributors, but their relative importance for pacemaking is still a matter of debate. This issue is complicated by the functional and morphological heterogeneity of SAN cells. In disaggregated SAN tissue preparations, different types of pacemaker cells are visually distinguishable by their unique sizes and shapes [6, 19, 30, 31]. Since these different cell types have distinct distribution patterns within the SAN [3, 30], it has been suggested that functional differences between SAN cells are important for the generation of electrical gradients and normal propagation of excitation from the central to peripheral SAN region. Indeed, Boyett and colleagues [12, 13, 16, 22] have reported cell size-dependent heterogeneity in action potential characteristics, density of various currents, gap junctions, and Ca^{2+}-handling proteins. In addition, cell shape-dependent characterization has revealed differences in the density and kinetics of the funny current (I_f) between spindle- and spider-shaped SAN cells [31]. Thus, cellular heterogeneity has been implicated in various mechanisms underlying the SAN pacemaker activity.

The sustained inward Na^+ current (I_{st}) has been identified in the SAN cells of rabbits, guinea pigs, rats, and mice

✉ Futoshi Toyoda
toyoda@belle.shiga-med.ac.jp

[1] Department of Physiology, Shiga University of Medical Science, Seta Tsukinowa, Otsu, Shiga 520-2192, Japan

[5, 7–9, 25, 28]. Because I_{st} is activated at low membrane potentials and provides a persistent inward current over the entire range of the slow diastolic depolarization, a contribution of I_{st} to the pacemaker activity has been suggested [21]. However, despite its physiological importance, the recording of I_{st} is rather infrequent and its heterogeneity among the various cells in the SAN has not been systematically investigated. Furthermore, molecular approaches have been hampered by the lack of identifiable molecular determinants for I_{st}. Recently, we have found that genetic ablation of the $Ca_V1.3$ L-type Ca^{2+} channel isoform results in abolition of I_{st} in mouse SAN cells [29], indicating that $Ca_V1.3$ is required for the generation of I_{st} in addition to L-type Ca^{2+} current ($I_{Ca,L}$). The mechanism as to how $Ca_V1.3$ could mediate two distinct currents remains to be elucidated. However, findings suggest that $Ca_V1.3$ can serve as a molecular marker to characterize distribution patterns of I_{st} in SAN cells. Here, we investigated the current density of I_{st} in morphologically different types of guinea pig SAN cells. Our extensive analysis shows a unique I_{st} distribution pattern that is associated with the cell shape and size, as well as the functional and transcriptional expression of $Ca_V1.3$-mediated $I_{Ca,L}$.

Methods

Ethical approval

All animal experiments were conducted in compliance with the protocol that was reviewed by the Institutional Animal Care and Use Committee, and approved by the President of Shiga University of Medical Science (Permit No. 2009-5-11).

SAN cell preparations

Single SAN cells from guinea pigs were isolated using an enzymatic dissociation method described previously [11, 20, 28, 32]. Adult Hartley guinea pigs (250 to 400 g body weight, $N = 16$) were deeply anesthetized by intraperitoneal administration of sodium pentobarbitone (80 mg kg^{-1}) and the chest cavity was opened under artificial ventilation. The ascending aorta was cannulated in situ and the heart was then excised and mounted on a Langendorff system. The heart was retrogradely perfused at 37 °C, initially for 4 min with normal Tyrode solution and then for 4 min with a nominally Ca^{2+}-free Tyrode solution. This was followed by 8–12 min perfusion with nominally Ca^{2+}-free Tyrode solution containing 0.4 mg ml^{-1} collagenase (Wako Pure Chemical Industries, Osaka, Japan). The SAN region, bordered by the crista terminalis, the intra-atrial septum, and cranial and caudal vena cava, was then dissected out and cut into small strips 0.5–1 mm wide. The strips of the SAN were subjected to another 20 min of digestion in nominally Ca^{2+}-free Tyrode solution containing 1.0 mg ml^{-1} collagenase (Wako) and 0.1 mg ml^{-1} elastase (Wako) in a shaking water bath at 37 °C. Finally, the SAN strips were transferred to ~5 ml of a high-K^+, low-Cl^- Kraftbrühe (KB) solution in a 35-mm culture dish, and single nodal cells were dispersed by mechanically agitating tissue strips with a fire-polished glass pipette. Cells were stored at 4 °C for later experiments on the day of dissociation.

Solutions and drugs

Normal Tyrode solution contained (mM) 140 NaCl, 5.4 KCl, 1.8 $CaCl_2$, 0.5 $MgCl_2$, 0.33 NaH_2PO_4, 5.5 glucose, and 5.0 HEPES (pH adjusted to 7.4 with NaOH). The nominally Ca^{2+}-free Tyrode solution used for the cell isolation procedure was prepared by simply omitting $CaCl_2$ from the normal Tyrode solution. The Cs^+-substituted, K^+-free Tyrode solution contained (mM) 140 NaCl, 5.4 CsCl, 1.8 $CaCl_2$, 0.5 $MgCl_2$, 0.33 NaH_2PO_4, 5.5 glucose, and 5.0 HEPES (pH adjusted to 7.4 with NaOH). The low-Ca^{2+}, Cs^+-substituted, K^+-free Tyrode solution contained (mM) 140 NaCl, 5.4 CsCl, 0.1 $CaCl_2$, 0.5 $MgCl_2$, 0.33 NaH_2PO_4, 5.5 glucose, and 5.0 HEPES (pH adjusted to 7.4 with NaOH). In some experiments, external Na^+ was totally replaced with N-methyl-D-glucamine-Cl ($NMDG^+$). Nicardipine and nifedipine (Sigma Chemical Co., St. Louis, MO, USA) were prepared as a 1 mM stock solution in DMSO and then diluted to a final concentration of 1 μM in the external solution. The Cs^+-rich pipette solution contained (mM) 125 CsOH, 20 tetraethylammonium chloride (TEA-Cl), 1.2 $CaCl_2$, 5 Mg-ATP (Sigma), 0.1 Li_2-GTP (Roche), 5 EGTA, and 10 HEPES (pH adjusted to 7.2 with aspartate). The concentration of free Ca^{2+} in the pipette solutions was calculated to be 33.2 nM. The KB solution for cell preservation contained (mM) 70 potassium glutamate, 30 KCl, 10 KH_2PO_4, 1 $MgCl_2$, 20 taurine, 0.3 EGTA, 10 glucose, and 10 HEPES (pH adjusted to 7.2 with KOH).

Whole-cell patch-clamp technique and data analysis

Isolated SAN cells were either current- or voltage-clamped using the whole-cell configuration of the patch-clamp technique [10] with an EPC-8 patch-clamp amplifier (HEKA Elektronik, Lambrecht, Germany). Patch electrodes were fabricated from glass capillaries (1.5 mm outer diameter, 0.9 mm inner diameter; Narishige Scientific Instrument Laboratory, Tokyo, Japan) using a Sutter P-97 microelectrode puller (Novato, CA, USA), and the tips were then fire-polished using a microforge. Patch electrodes had a resistance of 2.0–3.0 MΩ when filled with either the K^+-rich or Cs^+-rich pipette solution. A volume of dissociated cells was allowed to settle onto the glass bottom of a recording chamber (0.5 ml in volume) mounted on the stage of a Nikon TMD-300 inverted microscope equipped with a CCD digital camera (DS-Fi1, Nikon) to

capture images. The chamber was then continuously perfused at a constant rate of ~ 2 ml min^{-1} with normal Tyrode solution kept at 34–36 °C. Currents and voltages were digitized and voltage commands were generated through an LIH-1600 AD/DA interface (HEKA) controlled by PatchMaster software (Version 2.02, HEKA). All data were corrected for a liquid junction potential of − 10 mV between the aspartate-rich pipette solution and Tyrode solution. Cell membrane capacitance (C_m) was calculated for each cell by fitting the single exponential function to the decay of the capacitive transient resulting from 5 mV hyperpolarizing steps applied from a holding potential of − 50 mV [2].

One cell quantitative RT-PCR

cDNA generation from a single SAN cell was performed using a Takara CellAmp™ Whole Transcriptome Amplification Kit (Real Time) Ver. 2 (Takara Bio Inc., Japan) according to the manufacturer's instructions. Briefly, isolated single cells were harvested under a microscope and a glass pipette with a tip diameter of 10–30 μm, and immediately transferred into a 0.2 ml PCR tube containing 4.5-μl cell lysis buffer on ice. After cell lysis at 70 °C for 1.5 min, reverse transcription was performed at 42 °C for 5 min to synthesize cDNA. Poly(A) tails were then added to the 3′ end of cDNAs with terminal deoxynucleotidyl transferase, allowing non-selective pre-amplification of cDNA. The pre-amplified cDNA samples were diluted 20× and then used as a template for quantitative PCR assay. Real-time PCR was carried out in the LightCycler (Roche, Germany) and mRNA expression levels of specific genes were measured using a THUNDERBIRD SYBR qPCR mix (Toyobo, Japan). Primer sets used were as follows: $Ca_V1.2$ (NM_001172923) forward 5′- CCT CCA GAG AAG CCA TTC CCC-3′; reverse 5′- TGA GTT TCT CGC AGG ACT CGG-3′, $Ca_V1.3$ (XM_005008263) forward 5′- AAT GTG TGC ACC TGT ACC CTG G-3′; reverse 5′- CGA TGA TGT GTG AAA GGC CAC AG-3′, and beta-actin (NM_001172909) forward 5′- TGG ATC AGC AAG CAG GAG TAC G -3′; reverse 5′- TCG TTT TCT GCG CGC AAG TTA G-3′. Amplified products were confirmed by gel electrophoresis as well as by DNA sequencing.

Statistics

All averaged values presented are the mean ± S.E.M., and N and n indicate the number of animals and cells studied, respectively. Statistical comparisons were made using analysis of variance (ANOVA) followed by a post hoc Tukey HSD test, and the differences were considered significant at $P < 0.05$.

Results

Figure 1A shows micrographs of single SAN cells isolated from guinea pig hearts. According to morphological criteria described previously [6, 19, 30, 31], we identified three different types of nodal cells with distinct morphologies (spindle-, spider-, and elongated-shaped cells, Fig. 1a, i–iii), as well as the "atrial-like" cells (Fig. 1a, iv) that are widely distributed within the SAN [19, 30, 31]. In our preparations, the spindle and spider cells (assumed to be primary pacemaker cells [6, 31]) were smaller than the elongated and atrial-like cells (Fig. 1b), and constituted the predominant morphology among spontaneously beating cells. The elongated and atrial-like cells rarely displayed this spontaneous activity, but their beating rates were similar to those observed in spindle and spider cells (Fig. 1c). Both spontaneously beating and quiescent cells of each cell type were employed for the patch-clamp experiments. The current densities of I_f, I_{st}, and $I_{Ca,L}$ were examined in four distinct types of SAN cell. I_f was activated by a hyperpolarizing voltage-clamp pulse to − 120 mV from a holding potential of − 40 mV in the normal Tyrode solution (Fig. 2a, *left*), and then I_{st} and $I_{Ca,L}$ were elicited in the same cells by giving a two-step depolarizing command pulse from a holding potential of − 80 mV after blocking I_f by exposing the cell to the Cs^+-substituted, K^+-free Tyrode solution (Fig. 2a, *right*). I_{st} was determined as the dihydropyridine (nicardipine or nifedipine)-sensitive sustained inward current induced by an initial depolarizing step to − 50 mV. Even if $I_{Ca,L}$ was activated at this membrane potential, I_{st} could be isolated from $I_{Ca,L}$ since this current component was not appreciably affected by decreasing $[Ca^{2+}]_o$ to 0.1 mM, whereas fully-activated $I_{Ca,L}$ at − 10 mV was abolished. Conversely, I_{st} was largely reduced by removal of external Na^+ (Fig. 2b), indicating that Na^+ was the major current carrying ion. Figure 2c shows cumulative data plots for current densities in the four distinct types of SAN cell. I_f and $I_{Ca,L}$ were co-expressed in all SAN cell types tested. We did not find statistically significant differences in I_f and $I_{Ca,L}$ current densities between cell types. In contrast, I_{st} was barely detectable in atrial-like cells, but was evident in all other SAN cell types. The averaged I_{st} densities in spontaneously active spindle and spider cells were 1.03 ± 0.07 and 1.20 ± 0.10 pA pF^{-1}, respectively. These values were comparable to previous observations (~ 1.2 pA pF^{-1} in guinea pig SAN cells [7, 28]) but significantly larger than the values obtained from elongated cell types in the same SAN cell preparations (0.65 ± 0.07 pA pF^{-1}, $P < 0.05$). In addition, significantly smaller densities of I_{st} and $I_{Ca,L}$ were observed in non-beating cells, at least in spindle and spider cell types but not in elongated and atrial-like cells.

We examined the possible correlation between cell size and current densities for various ionic currents as previously described in rabbit SAN cells [3]. A significant negative correlation between the I_{st} density and cell size (membrane capacitance)

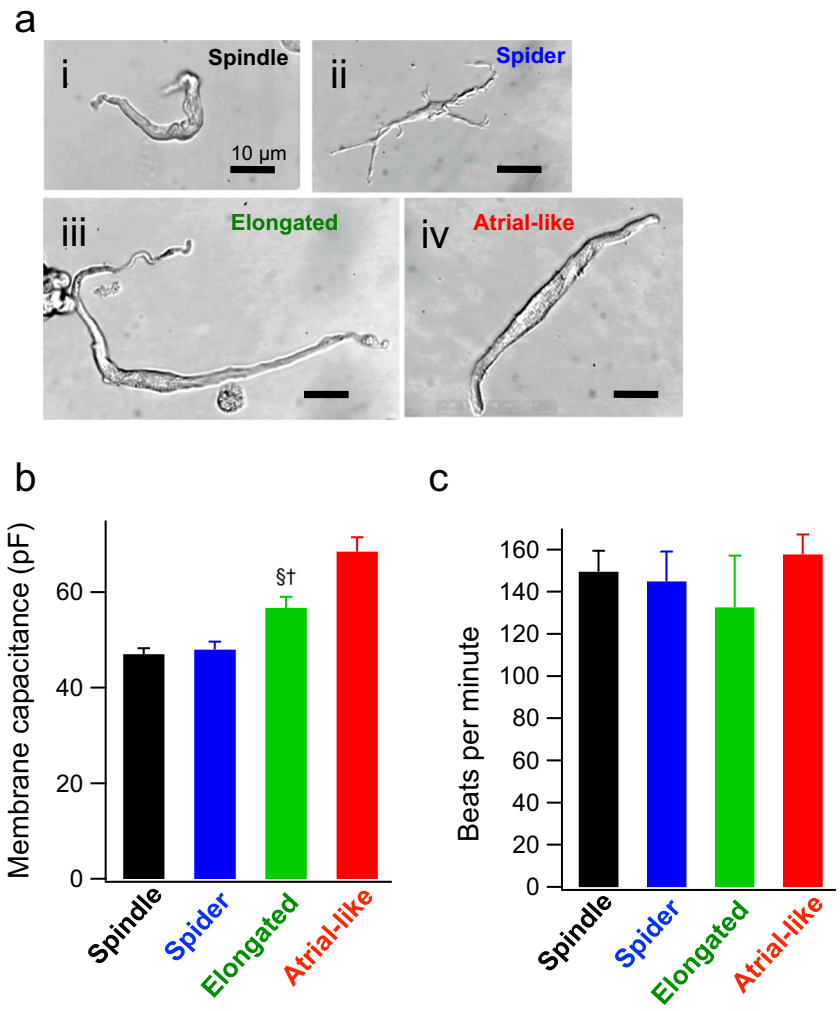

Fig. 1 The density of I_f, I_{st}, and $I_{Ca,L}$ in different types of guinea pig SAN cells. **a**. Representative microscopic images of single SAN cells isolated from guinea pig hearts; the spindle-shaped cell (*i*), the spider-shaped cell (*ii*), the elongated spindle-shaped cell (*iii*), and the atrial-like cell (*iv*). **b**. Averaged C_m in the spindle ($n = 23$, $N = 10$), spider ($n = 15$, $N = 11$), elongated ($n = 11$, $N = 5$), and atrial-like cells ($n = 9$, $N = 3$). §, †, and ¶, $P < 0.05$ for versus the spindle cell, the spider cell and the elongated cell, respectively (ANOVA and post hoc Tukey HSD test). **c**. Spontaneous beating rate (beats/min) of distinct cell types as assessed by visual observation

was found ($r = -0.703$, $P < 0.001$, Fig. 3), whereas the densities of $I_{Ca,L}$ and I_f were independent of cell size. It should be noted that the correlation between the I_{st} density and cell size was not significant within a given cell type (spindle, $r = -0.033$, $P = 0.903$; spider, $r = 0.215$, $P = 0.610$; elongated, $r = -0.155$, $P = 0.740$; atrial-like, $r = 0.797$, $P = 0.106$), suggesting that the I_{st} density is still associated with cell types rather than cell size.

Combined recordings of I_f, I_{st} and $I_{Ca,L}$ from each cell allowed us to investigate relationships between these currents. In Fig. 4, scatter plots of current densities in each cell type are drawn for different pairs of I_f, I_{st}, and $I_{Ca,L}$. In this analysis, values obtained from non-beating cells were also included to allow linear regressions to be applied through a wide range of current densities. As shown in Fig. 4a and c, neither I_{st} nor $I_{Ca,L}$ exhibited a significant correlation with I_f in any cell type. On the other hand, a significant positive correlation between I_{st} and $I_{Ca,L}$ was found in all cell types other than atrial-like cells (spindle, $r = 0.699$, $P < 0.001$; spider, $r = 0.694$, $P < 0.001$; and elongated, $r = 0.532$, $P < 0.05$, Fig. 4b). Interestingly, the slope of the regression line was similar for spindle and spider cells, while it was reduced in the elongated cell type. No correlation was noted for atrial-like cells due to the absence of I_{st} in this cell type.

It is now generally accepted that $I_{Ca,L}$ in SAN cells is composed of two separate current components mediated by two different pore-forming alpha subunits, $Ca_V1.2$ and $Ca_V1.3$ [17, 34]. We thus hypothesized that the composition of $Ca_V1.2$ and $Ca_V1.3$ subunits in mediating SAN $I_{Ca,L}$ might affect the relationship between I_{st} and $I_{Ca,L}$. Since $Ca_V1.3$-mediated $I_{Ca,L}$ activates at more negative voltages than $Ca_V1.2$-mediated $I_{Ca,L}$ [15], the relative contribution of $Ca_V1.2$ and $Ca_V1.3$ subunits could be approximated by the voltage-dependence of $I_{Ca,L}$. In the experiment shown in Fig. 5a, $I_{Ca,L}$ was recorded in distinct types of guinea pig SAN cells under conditions where other time- and voltage-dependent currents were minimized; i.e., I_{st} and I_{Na} were eliminated by total replacement of extracellular Na^+ with equimolar amount of $NMDG^+$, and $I_{Ca,T}$ was inactivated by a holding potential of −60 mV [17]. There was no obvious difference between cell types in the voltage threshold for $I_{Ca,L}$ activation (~−40 mV). However, the voltage

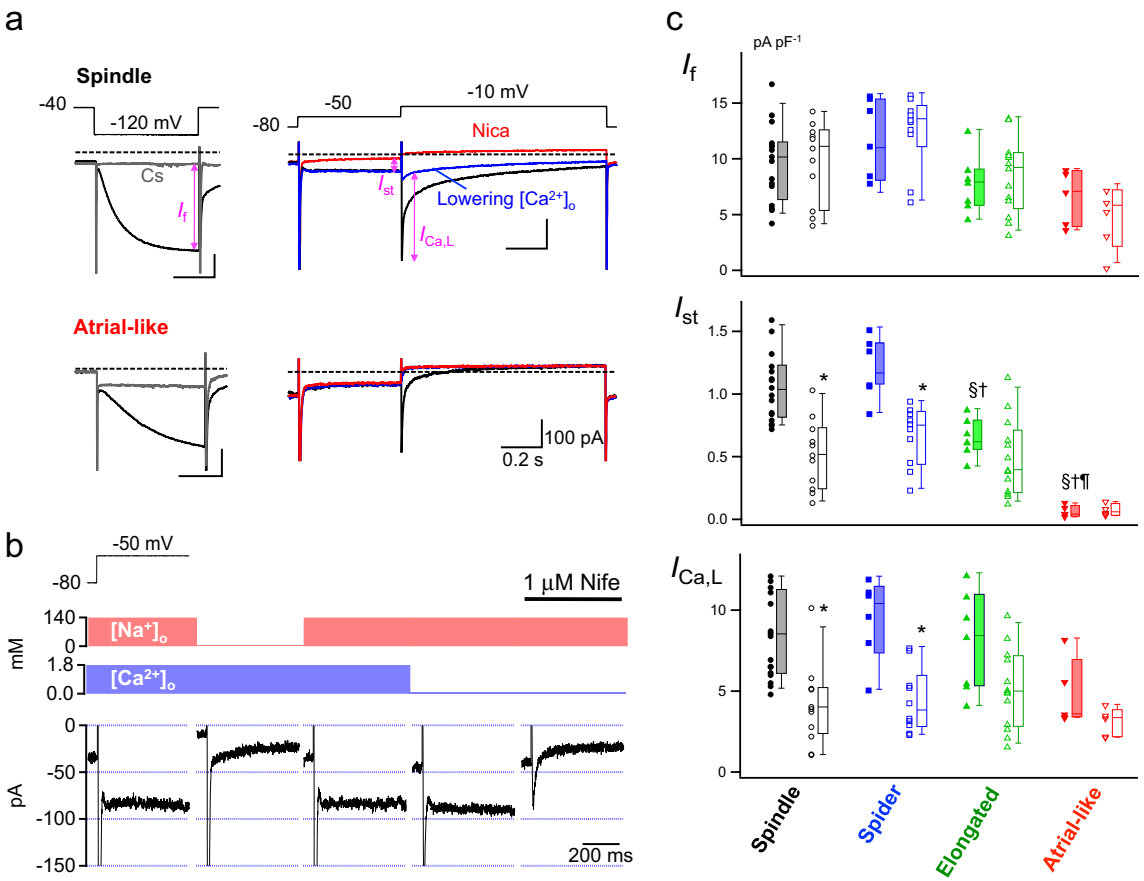

Fig. 2 The density of I_f, I_{st}, and $I_{Ca,L}$ in different types of guinea pig SAN cells. **a**. Current recordings in single spindle-shaped (a) and atrial-like (b) SAN cells. The cell was initially voltage-clamped at a holding potential of − 40 mV and I_f was elicited by a 1-s hyperpolarizing pulse to − 120 mV (left). After blocking I_f by perfusing the cell with the Cs^+-substituted, K^+-free Tyrode solution, the holding potential was switched to − 80 mV and a two-step command pulse (top panel) was given to activate I_{st} and $I_{Ca,L}$ (right). I_{st} was manifested after the fast inactivating transient inward current (I_{Na} and/or $I_{Ca,T}$) during a 0.5-s depolarizing pulse to − 50 mV. $I_{Ca,L}$ was elicited by a following 1-s depolarization to − 10 mV. Current recordings under control condition (black trace), during exposure to the low-Ca^{2+}, Cs^+-substituted, K^+-free Tyrode solution (blue trace) and after application of 1 μM nicardipine are superimposed. **b.** Current traces of I_{st} elicited from a spindle cell by a depolarizing pulse to − 50 mV. I_{st} is largely eliminated by omitting external Na^+ but not by lowering external Ca^{2+}. **c**. Dot and box plots of I_f, I_{st}, and $I_{Ca,L}$ densities in the spindle cells (black), the spider cells (blue), the elongated spindle cells (green), and the atrial-like cells (red). For each cell type, data from the spontaneous active cell (filled dots) and the non-beating cell (open dots) are plotted separately. Large symbol with bar indicates mean ± S.E.M. Asterisks indicate significant difference ($P < 0.05$, Student t test) between spontaneously active cells and non-beating cells. §, †, and ¶, $P < 0.05$ for versus the spindle cell, the spider cell, and the elongated cell, respectively (ANOVA and post hoc Tukey HSD test)

giving maximum $I_{Ca,L}$ varied between the cell types; for example, − 17 mV in spindle cells vs. +1 mV in atrial-like cells, Fig. 5a and b). In Fig. 5c, the averaged conductance (G) densities were calculated and plotted as a function of the pulse potentials in each cell type, which were fitted with smooth curves derived from the Boltzmann equation. There was no statistical difference between cell types in the maximal conductance (G_{max}) density (Fig. 5c, *upper*). On the other hand, as indicated by normalized conductance (G/G_{max})-voltage curves (Fig. 5c, *lower*), the half-maximal activation voltages ($V_{0.5}$) obviously varied across different cell types. The $V_{0.5}$ in the spindle, spider, and elongated cells were − 31.63 ± 1.15 mV ($n = 4$, $N = 2$), − 27.7 ± 2.19 mV ($n = 5$, $N = 2$), and − 20.16 ± 2.86 mV ($n = 4$, $N = 2$), respectively. These values were significantly more negative than − 12.36 ± 4.47 mV in atrial-like cells ($n = 4$, $N = 2$, $P < 0.05$). It is thus suggested that the relative contribution of $Ca_V1.2$ and $Ca_V1.3$ isoforms to I_{CaL} differs in different cell types. As a lower $V_{0.5}$ of $I_{Ca,L}$ indicates a larger contribution of $Ca_V1.3$, the results suggest that $Ca_V1.3$-mediated $I_{Ca,L}$ is more prominent in spindle and spider cells compared to elongated or atrial-like cells. Finally, to substantiate this view, single spindle and atrial-like cells were individually harvested under microscopy using a glass pipette and examined for their relative expression of $Ca_V1.2$ and $Ca_V1.3$ by one cell quantitative RT-PCR analysis (Fig. 5d). Although not statistically significant due to large variability, there was a trend which suggested that the mRNA level of $Ca_V1.2$ was higher in atrial-like cells, whereas $Ca_V1.3$ mRNA was more abundant in spindle cells. The expression ratio of $Ca_V1.3$ to $Ca_V1.2$ was significantly higher in spindle cells compared with atrial-like cells ($P < 0.05$).

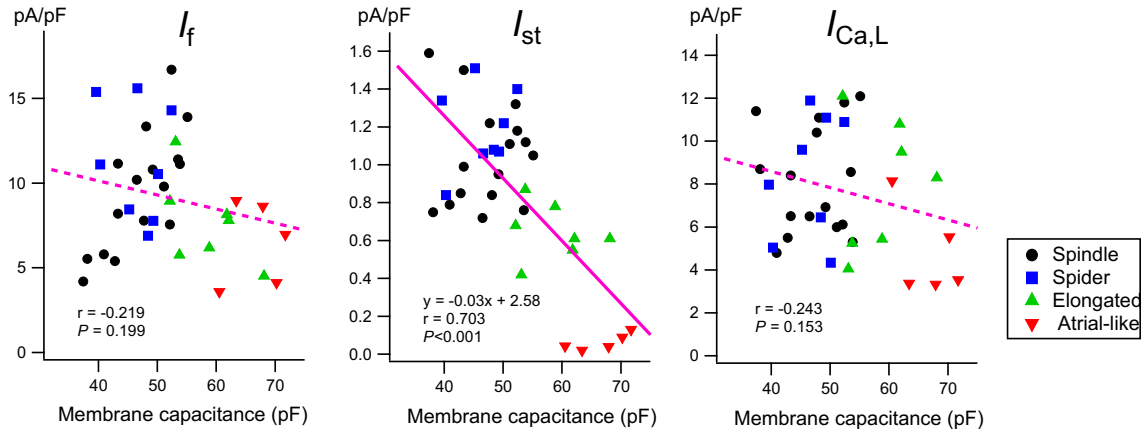

Fig. 3 The relationship between the cell size and the current density. Scatter plot of the cell size versus the current densities of I_f (left), I_{st} (middle), and $I_{Ca,L}$ (right). Data were obtained for the spontaneously active spindle cell (black circle), the spider cell (blue square), the elongated spindle cell (green upward triangle), and the atrial-like cell (red downward triangle). Solid and dashed lines indicate the least square fit with and without a statistically significant trend, respectively

Discussion

The present study has provided the first detailed characterization of I_{st} heterogeneity in guinea pig SAN cells. Consistent with observations from previous work by Noma's group [7, 8, 25], our results show that the presence of I_{st} is closely associated with cell morphology. Indeed, I_{st} can be recorded in spontaneously active cells with typical pacemaker cell morphologies, namely spindle- and spider-shaped cells. By contrast, this current is scarcely detectable in larger-sized atrial-like cells even when they exhibit I_f, a conventional electrophysiological hallmark of SAN cells. Notably, this study uncovered a positive correlation between I_{st} and $I_{Ca,L}$ current densities, which was specifically observed in spindle and spider cells. These cells display $Ca_V1.3$-mediated $I_{Ca,L}$ which activates at more negative voltages than recorded in atrial-like cells. It is thus suggested that the functional expression of I_{st} is correlated with that of $Ca_V1.3$-mediated rather than $Ca_V1.2$-mediated $I_{Ca,L}$. In this regard, we have recently demonstrated that $Ca_V1.3$ gene ablation in mice results in the abolition of I_{st} in SAN cells [29]. Thus, our findings support the emerging concept that the $Ca_V1.3$ L-type channel is a molecular component required for the generation of I_{st} in SAN cells.

Cell morphology is an important criterion for identifying SAN pacemaker cells. In general, the spindle- and spider-shaped cells are assumed to be the primary pacemaker cell types exhibiting regular rhythmic spontaneous activity after enzymatic dissociation [3, 6]. In addition, these small cells are densely distributed in the center (leading pacemaker site) of SAN [30]. On the other hand, the large-sized elongated cells are known to be abundant in the area adjacent to the crista terminalis [30], suggesting that this cell type belongs to the intermediate or transitional (peripheral) class of SAN cells. Therefore, the higher current density of I_{st} in spindle and spider cells compared to elongated cells suggests that I_{st} plays a specific role in primary pacemaker cells. In disaggregated cell preparations, rod-shaped atrial-like cells abound. These myocytes are distributed over a wide area within the SAN [19, 30]. The atrial-like cell appears to be different from working atrial myocytes because some of the cells display spontaneous activity. In addition, our patch-clamp recordings revealed that most of the atrial-like cells exhibit I_f. However, the complete absence of I_{st} in the atrial-like cells indicates that I_{st} is not involved in the pacemaker mechanism in this cell type. Considering the unique biophysical and pharmacological properties of I_{st}, the cell type-dependent distribution of this current may be at least partly responsible for regional differences in action potential characteristics as well as differential sensitivities to dihydropyridines and autonomic transmitters in the SAN [14, 33].

Our cell preparations contained a large number of non-beating cells with typical spindle and spider cell morphologies. One possible explanation for the inability to generate spontaneous action potentials may be a significantly lower density of I_{st} and $I_{Ca,L}$ in these cells. In support of this, our preliminary experiments showed that many of these quiescent cells initiate beating after exposure to a dihydropyridine agonist Bay-K8644 that can potentiate both I_{st} and $I_{Ca,L}$ [7]. Ca_V1-$I_{Ca,L}$ channel proteins on the membrane experience a high turnover with a half-life as short as 3 h [4], whereas a much longer half-life of > 2 days is reported for the HCN-I_f channel [24]. It is therefore possible that rapid downregulation of I_{st} and $I_{Ca,L}$ rather than mechanical damage during cell dissociation procedures is involved in impaired spontaneous activity in isolated SAN cells.

In contrast to the limited distribution of I_{st} and I_f in pacemaker cells, $I_{Ca,L}$ is commonly present in all cardiomyocytes and plays a fundamental role in electrical and contractile activities. However, the molecular background of $I_{Ca,L}$ varies between different cardiac regions. $Ca_V1.2$ is uniformly

expressed across all regions of the heart, whereas $Ca_V1.3$ is nearly absent in ventricles but is more specifically expressed in the conduction system including the SAN [17, 26]. Furthermore, the present study has revealed that, even in the SAN region, the composition of $Ca_V1.2$- and $Ca_V1.3$-mediated $I_{Ca,L}$ is heterogeneous, suggesting that $I_{Ca,L}$ differentially contributes to the pacemaker activity in distinct SAN cell types. In SAN cells, $Ca_V1.2$-mediated $I_{Ca,L}$ is responsible for the upstroke of action potential, while $Ca_V1.3$-mediated $I_{Ca,L}$ activates at more negative potentials, thereby contributing to diastolic depolarization [17]. In fact, impaired $Ca_V1.3$ channel function results in severe sinus bradycardia in mouse and human hearts [1, 17, 23, 34]. Thus, our findings that $Ca_V1.3$-mediated $I_{Ca,L}$ is more abundant in spindle- or spider-shaped primary pacemaker cells than atrial-like cells are in good agreement with the well-accepted concept that $Ca_V1.3$-mediated $I_{Ca,L}$ plays a pivotal role in the normal heart rhythm.

We have recently shown that $Ca_V1.3$ acts as an essential molecular determinant for the induction of I_{st} in mouse SAN cells [29], providing evidence for an additional role of $Ca_V1.3$ in heart automaticity. This view is further strengthened by the present study which revealed the quantitative relationship between functional levels of I_{st} and $Ca_V1.3$-mediated $I_{Ca,L}$. Although elucidating the molecular mechanism allowing $Ca_V1.3$ to mediate both Ca^{2+} and Na^+ currents is still challenging, the present study indicates that two distinct currents, $I_{Ca,L}$ and I_{st}, are synchronously regulated by the expression of $Ca_V1.3$. I_{st} provides a persistent inward Na^+ current over the

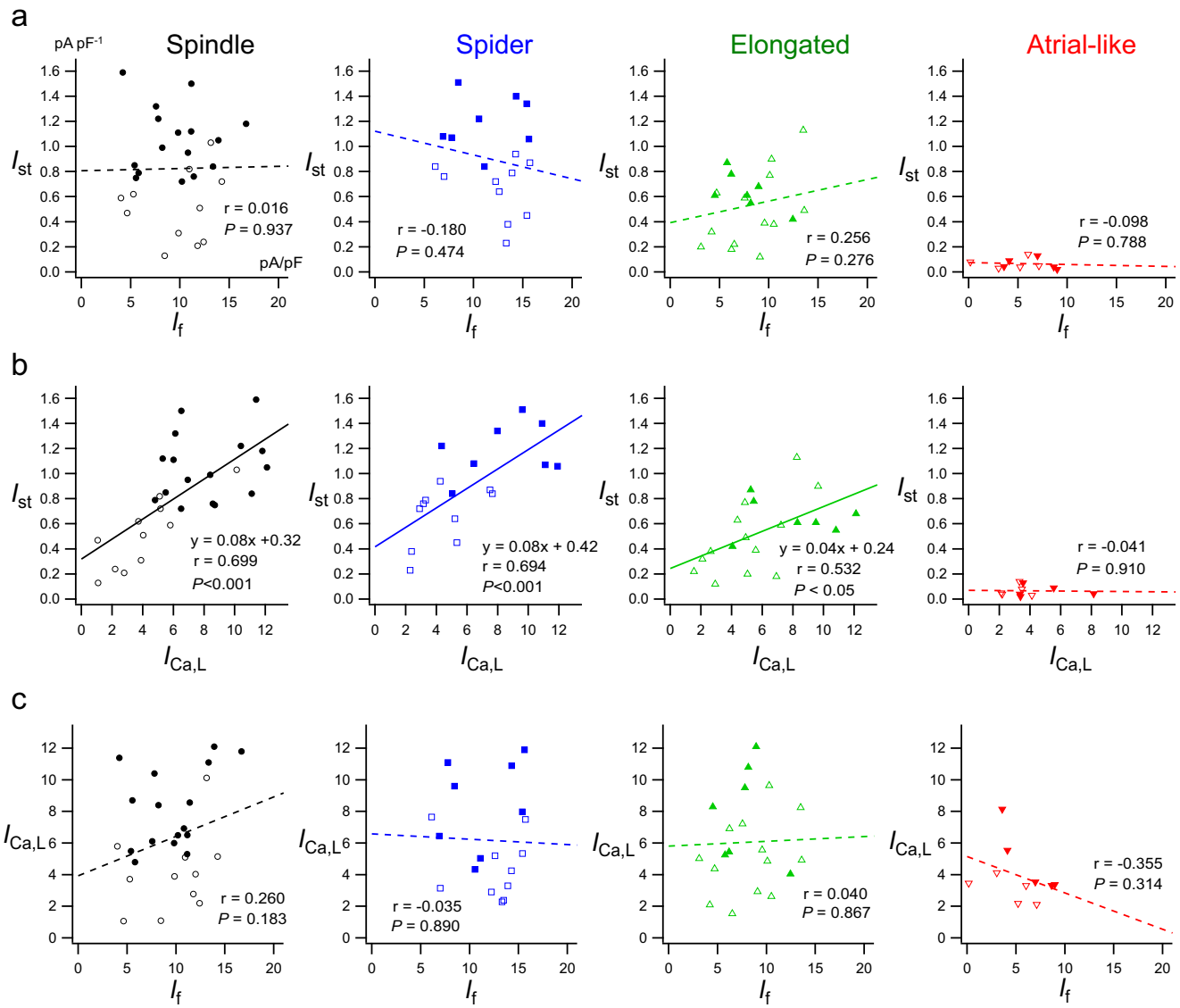

Fig. 4 Correlation between the densities of I_f, I_{st}, and $I_{Ca,L}$ in guinea pig SAN cells. **a**. Scatter plots of I_f versus I_{st} density in spindle cells (black), spider cells (blue), elongated spindle cells (green), and the atrial-like cells (red). Lines (solid or dotted) in each cell type indicate the least squares fit to the combined data points from the spontaneous active cell (filled dot) and the non-beating cell (open dot). **b**. Scatter plots of the $I_{Ca,L}$ density versus the I_{st} density in distinct cell types. **c**. Scatter plots of the I_f density versus the $I_{Ca,L}$ density in distinct cell types

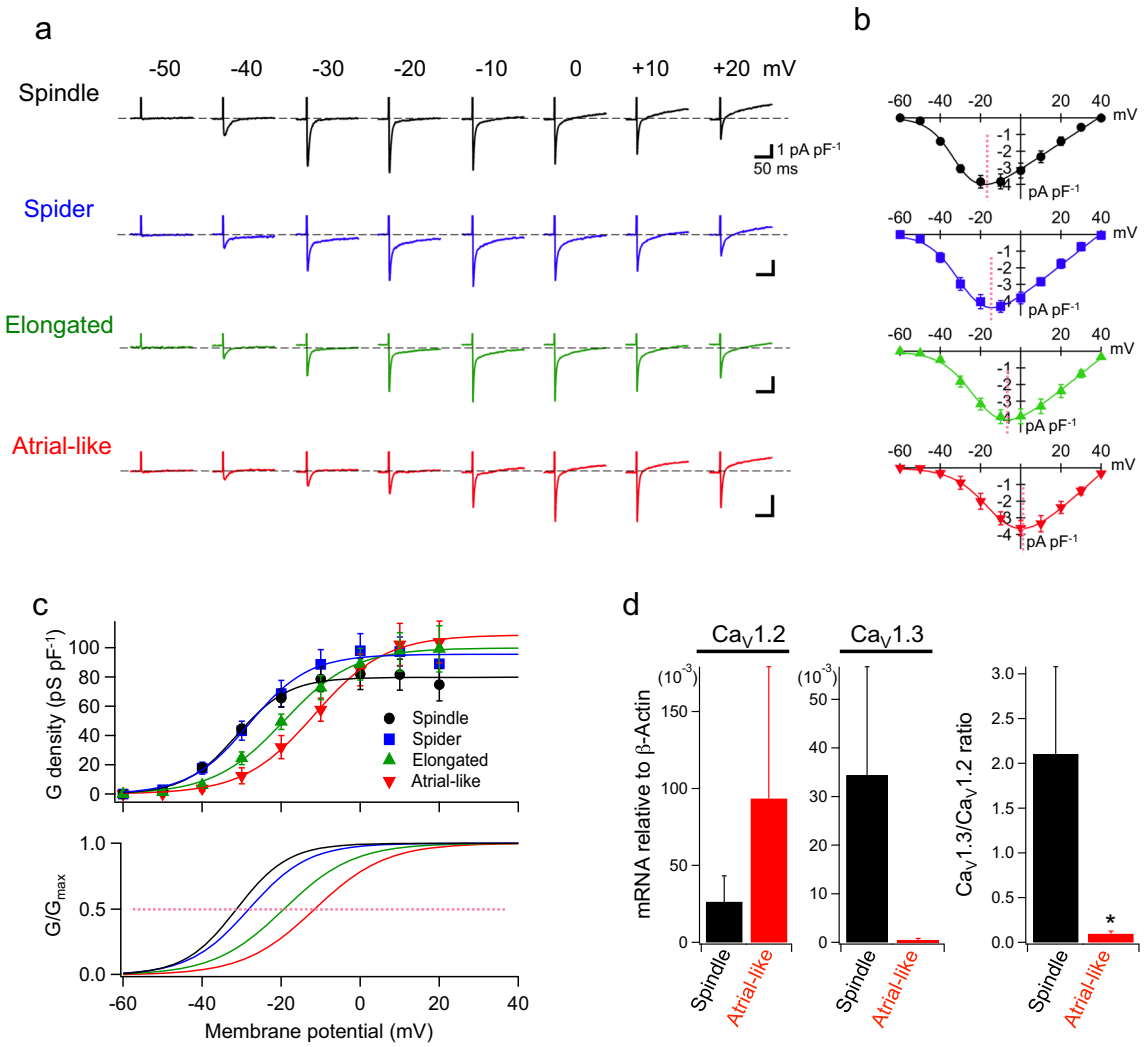

Fig. 5 Cell type-dependent molecular compositions of $I_{Ca,L}$ in guinea pig SAN cells. **a**. $I_{Ca,L}$ recordings in the spindle (black), spider (blue), elongated (green), and atrial-like cells (red). Currents were elicited by depolarizing steps to various test potentials from a holding potential of − 60 mV. To eliminate I_{Na} and I_{st}, Na^+ in the bath solution was totally replaced with NMDG. **b.** Averaged current-voltage relationships of $I_{Ca,L}$ in each cell type. The dotted line indicates the voltage giving peak inward current. Data were pooled from four or five experiments and are shown as mean ± S.E.M. **c.** Averaged conductance (G) density-voltage relationships (*upper*), fitted by the Boltzmann equation: $G = G_{max}/\{1 + \exp.[(V_{0.5} - V)/s]\}$, where G is the conductance density, V is the membrane potential, G_{max} is the cell maximum conductance density, $V_{0.5}$ is the voltage for half current activation, and s is the slope factor of the Boltzmann term. The *lower* graph illustrates normalized conductance (G/G_{max})-voltage curves in each cell type. **d.** $Ca_V1.2$ and $Ca_V1.3$ mRNA expression in spindle (black, $n = 11$, $N = 2$) and atrial-like cells (red, $n = 12$, $N = 2$). Asterisk indicates a significant difference ($P < 0.05$, Student t test)

entire range of the diastolic depolarization, while $Ca_V1.3$-mediated $I_{Ca,L}$ is activated in the diastolic depolarization and generates Ca^{2+} influx that controls ryanodine receptor-dependent Ca^{2+} release [27]. In addition, both I_{st} and $Ca_V1.3$-mediated $I_{Ca,L}$ are enhanced by β-adrenergic stimulation [29], suggesting that these currents coordinately contribute to the sympathetic regulation of the SAN pacemaker activity.

Acknowledgements The authors are grateful to Dr. Matteo E. Mangoni and Dr. Jeorg Striessnig for fruitful discussions and encouragement.

Author contributions F.T., D. W-G., and H.M. designed the study. F.T. performed all experiments and analyzed the data. F.T. drafted the manuscript and all authors critically revised it for technical and important contents.

Funding The project was supported by the Grant-in-Aid for Scientific Research (C) 23590258, 26460295 and 17K08537 from the Japan Society for the Promotion of Science (to F.T.).

References

1. Baig SM, Koschak A, Lieb A, Gebhart M, Dafinger C, Nürnberg G, Ali A, Ahmad I, Sinnegger-Brauns MJ, Brandt N, Engel J, Mangoni ME, Farooq M, Khan HU, Nurnberg P, Striessnig J, Bolz HJ (2011) Loss of $Ca_V1.3$ (*CACNA1D*) function in a human

channelopathy with bradycardia and congenital deafness. Nat Neurosci 14(1):77–84. https://doi.org/10.1038/nn.2694
2. Benitah JP, Gomez AM, Bailly P, Da Ponte JP, Berson G, Delgado C, Lorente P (1993) Heterogeneity of the early outward current in ventricular cells isolated from normal and hypertrophied rat hearts. J Physiol 469(1):111–138. https://doi.org/10.1113/jphysiol.1993.sp019807
3. Boyett MR, Honjo H, Kodama I (2000) The sinoatrial node, a heterogeneous pacemaker structure. Cardiovasc Res 47(4):658–687. https://doi.org/10.1016/S0008-6363(00)00135-8
4. Chien AJ, Zhao X, Shirokov RE, Puri TS, Chang CF, Sun D, Rios E, Hosey MM (1995) Roles of a membrane-localized beta subunit in the formation and targeting of functional L-type Ca^{2+} channels. J Biol Chem 270(50):30036–30044
5. Cho HS, Takano M, Noma A (2003) The electrophysiological properties of spontaneously beating pacemaker cells isolated from mouse sinoatrial node. J Physiol 550(1):169–180. https://doi.org/10.1113/jphysiol.2003.040501
6. Denyer JC, Brown HF (1990) Rabbit sino-atrial node cells: isolation and electrophysiological properties. J Physiol 428(1):405–424. https://doi.org/10.1113/jphysiol.1990.sp018219
7. Guo J, Mitsuiye T, Noma A (1997) The sustained inward current in sino-atrial node cells of guinea-pig heart. Pflugers Arch 433(4):390–396. https://doi.org/10.1007/s004240050293
8. Guo J, Ono K, Noma A (1995) A sustained inward current activated at the diastolic potential range in rabbit sino-atrial node cells. J Physiol 483(1):1–13. https://doi.org/10.1113/jphysiol.1995.sp020563
9. Guo J, Ono K, Noma A (1996) Monovalent cation conductance of the sustained inward current in rabbit sinoatrial node cells. Pflugers Arch 433(1-2):209–211. https://doi.org/10.1007/s004240050269
10. Hamill OP, Marty A, Neher E, Sakmann B, Sigworth FJ (1981) Improved patch-clamp techniques for high-resolution current recording from cells and cell-free membrane patches. Pflugers Arch 391(2):85–100. https://doi.org/10.1007/BF00656997
11. Himeno Y, Toyoda F, Satoh H, Amano A, Cha CY, Matsuura H, Noma A (2011) Minor contribution of cytosolic Ca^{2+} transients to the pacemaker rhythm in guinea pig sinoatrial node cells. Am J Physiol Heart Circ Physiol 300(1):H251–H261. https://doi.org/10.1152/ajpheart.00764.2010
12. Honjo H, Boyett MR, Coppen SR, Takagishi Y, Opthof T, Severs NJ, Kodama I (2002) Heterogeneous expression of connexins in rabbit sinoatrial node cells: correlation between connexin isotype and cell size. Cardiovasc Res 53(1):89–96. https://doi.org/10.1016/S0008-6363(01)00421-7
13. Honjo H, Boyett MR, Kodama I, Toyama J (1996) Correlation between electrical activity and the size of rabbit sino-atrial node cells. J Physiol 496(3):795–808. https://doi.org/10.1113/jphysiol.1996.sp021728
14. Kodama I, Nikmaram MR, Boyett MR, Suzuki R, Honjo H, Owen JM (1997) Regional differences in the role of the Ca^{2+} and Na^{+} currents in pacemaker activity in the sinoatrial node. Am J Phys 272:H2793–H2806
15. Koschak A, Reimer D, Huber I, Grabner M, Glossmann H, Engel J, Striessnig J (2001) α_{1D} ($Ca_v1.3$) subunits can form L-type Ca^{2+} channels activating at negative voltages. J Biol Chem 276(25):22100–22106. https://doi.org/10.1074/jbc.M101469200
16. Lei M, Honjo H, Kodama I, Boyett MR (2001) Heterogeneous expression of the delayed-rectifier K^{+} currents $i_{K,r}$ and $i_{K,s}$ in rabbit sinoatrial node cells. J Physiol 535(3):703–714. https://doi.org/10.1111/j.1469-7793.2001.t01-1-00703.x
17. Mangoni ME, Couette B, Bourinet E, Platzer J, Reimer D, Striessnig J, Nargeot J (2003) Functional role of L-type $Ca_v1.3$ Ca^{2+} channels in cardiac pacemaker activity. Proc Natl Acad Sci U S A 100(9):5543–5548. https://doi.org/10.1073/pnas.0935295100
18. Mangoni ME, Nargeot J (2008) Genesis and regulation of the heart automaticity. Physiol Rev 88(3):919–982. https://doi.org/10.1152/physrev.00018.2007
19. Mangoni ME, Nargeot J (2001) Properties of the hyperpolarization-activated current (I_f) in isolated mouse sino-atrial cells. Cardiovasc Res 52(1):51–64. https://doi.org/10.1016/S0008-6363(01)00370-4
20. Matsuura H, Ehara T, Ding WG, Omatsu-Kanbe M, Isono T (2002) Rapidly and slowly activating components of delayed rectifier K^{+} current in guinea-pig sino-atrial node pacemaker cells. J Physiol 540(3):815–830. https://doi.org/10.1113/jphysiol.2001.016741
21. Mitsuiye T, Shinagawa Y, Noma A (2000) Sustained inward current during pacemaker depolarization in mammalian sinoatrial node cells. Circ Res 87(2):88–91. https://doi.org/10.1161/01.RES.87.2.88
22. Musa H, Lei M, Honjo H, Jones SA, Dobrzynski H, Lancaster MK, Takagishi Y, Henderson Z, Kodama I, Boyett MR (2002) Heterogeneous expression of Ca^{2+} handling proteins in rabbit sinoatrial node. J Histochem Cytochem 50(3):311–324. https://doi.org/10.1177/002215540205000303
23. Platzer J, Engel J, Schrott-Fischer A, Stephan K, Bova S, Chen H, Zheng H, Striessnig J (2000) Congenital deafness and sinoatrial node dysfunction in mice lacking class D L-type Ca^{2+} channels. Cell 102(1):89–97. https://doi.org/10.1016/S0092-8674(00)00013-1
24. Santoro B, Wainger BJ, Siegelbaum SA (2004) Regulation of HCN channel surface expression by a novel C-terminal protein-protein interaction. J Neurosci 24(47):10750–10762. https://doi.org/10.1523/JNEUROSCI.3300-04.2004
25. Shinagawa Y, Satoh H, Noma A (2000) The sustained inward current and inward rectifier K^{+} current in pacemaker cells dissociated from rat sinoatrial node. J Physiol 523(3):593–605. https://doi.org/10.1111/j.1469-7793.2000.t01-2-00593.x
26. Sinnegger-Brauns MJ, Hetzenauer A, Huber IG, Renstrom E, Wietzorrek G, Berjukov S, Cavalli M, Walter D, Koschak A, Waldschutz R, Hering S, Bova S, Rorsman P, Pongs O, Singewald N, Striessnig JJ (2004) Isoform-specific regulation of mood behavior and pancreatic beta cell and cardiovascular function by L-type Ca^{2+} channels. J Clin Invest 113(10):1430–1439. https://doi.org/10.1172/JCI20208
27. Torrente AG, Mesirca P, Neco P, Rizzetto R, Dubel S, Barrere C, Sinegger-Brauns M, Striessnig J, Richard S, Nargeot J, Gomez AM, Mangoni ME (2016) L-type Cav1.3 channels regulate ryanodine receptor-dependent Ca^{2+} release during sino-atrial node pacemaker activity. Cardiovasc Res 109(3):451–461. https://doi.org/10.1093/cvr/cvw006
28. Toyoda F, Ding WG, Matsuura H (2005) Responses of the sustained inward current to autonomic agonists in guinea-pig sino-atrial node pacemaker cells. Br J Pharmacol 144(5):660–668. https://doi.org/10.1038/sj.bjp.0706101
29. Toyoda F, Mesirca P, Dubel S, Ding WG, Striessnig J, Mangoni ME, Matsuura H (2017) $Ca_V1.3$ L-type Ca^{2+} channel contributes to the heartbeat by generating a dihydropyridine-sensitive persistent Na^{+} current. Sci Rep 7(1):7869. https://doi.org/10.1038/s41598-017-08191-8
30. Verheijck EE, Wessels A, van Ginneken AC, Bourier J, Markman MW, Vermeulen JL, de Bakker JM, Lamers WH, Opthof T, Bouman LN (1998) Distribution of atrial and nodal cells within the rabbit sinoatrial node: models of sinoatrial transition. Circulation 97(16):1623–1631. https://doi.org/10.1161/01.CIR.97.16.1623
31. Wu J, Schuessler RB, Rodefeld MD, Saffitz JE, Boineau JP (2001) Morphological and membrane characteristics of spider and spindle cells isolated from rabbit sinus node. Am J Physiol Heart Circ Physiol 280(3):H1232–H1240
32. Xie Y, Ding WG, Matsuura H (2015) Ca^{2+}/calmodulin potentiates I_{Ks} in sinoatrial node cells by activating Ca^{2+}/calmodulin-dependent protein kinase II. Pflugers Arch 467(2):241–251. https://doi.org/10.1007/s00424-014-1507-1

33. Yamamoto M, Honjo H, Niwa R, Kodama I (1998) Low-frequency extracellular potentials recorded from the sinoatrial node. Cardiovasc Res 39(2):360–372. https://doi.org/10.1016/S0008-6363(98)00091-1

34. Zhang Z, Xu Y, Song H, Rodriguez J, Tuteja D, Namkung Y, Shin HS, Chiamvimonvat N (2002) Functional roles of $Ca_v1.3$ (α_{1D}) calcium channel in sinoatrial nodes: insight gained using gene-targeted null mutant mice. Circ Res 90(9):981–987. https://doi.org/10.1161/01.RES.0000018003.14304.E2